Cryogenic MOSFET Threshold Voltage Model

Arnout Beckers, Farzan Jazaeri, and Christian Enz

Integrated Circuits Laboratory (ICLAB), Ecole Polytechnique Fédérale de Lausanne, Neuchâtel, Switzerland

Abstract—**This paper presents a physics-based model for the threshold voltage in bulk MOSFETs valid from room down to cryogenic temperature (4.2 K). The proposed model is derived from Poisson's equation including bandgap widening, intrinsic carrier-density scaling, and incomplete ionization. We demonstrate that accounting for incomplete ionization in the expression of the threshold voltage is critical for an accurate estimation of the current. The model is validated with our experimental results from nMOSFETs of a 28-nm CMOS process. The developed model is a key element for a cryo-CMOS compact model and can serve as a guide to optimize processes for high-performance cryo-computing and ultra-low-power quantum computing.**

I. Introduction

Remarkable progress towards a silicon quantum computer in recent years has attracted attention to the operation of VLSI technologies at deep-cryogenic temperatures (< 10 K) [1]–[6]. Dedicated cryo-CMOS circuits can reduce the overhead associated with the initialization, manipulation, coupling, and read-out of qubits. The power consumption of the CMOS circuits envisioned for qubit control is severely limited ($\approx$ 1 W at 4.2 K). At the same time, the circuits need to meet sharp timing constraints on the control pulses applied to the qubits. This delicate trade-off between power consumption and performance at cryogenic temperatures ultimately asks for an accurate model of the MOSFET threshold voltage (V_T).

Besides quantum computing, temperature scaling can also provide a performance booster for conventional computing applications, if harnessed carefully. As shown in Fig. 1, cryogenic operation does *not* improve the on-state current (I_{ON}) of small commercial devices at the maximum supply voltage (V_{DD}). Furthermore, the available overdrive voltage ($V_{DD} - V_T$) is reduced by the substantial increase of V_T down to cryogenic temperatures ($\Delta V_T \approx 0.1 - 0.2$ V). However, there is room for improvement since the leakage current is extremely low at cryogenic temperature. The $I - V$ curve can thus be shifted by selecting a custom work function difference and/or doping, hence supporting a larger $V_{DD} - V_T$ for high performance applications or a scaled V_{DD} for ultra-low power applications.

Importantly, both technology optimization and the use of commercial devices require that V_T can be accurately predicted. Since the MOSFET turns on over a few millivolts at cryogenic temperatures, a small mis-prediction of V_T leads to orders of magnitude difference in the drain current. To arrive at the most accurate model for V_T, incomplete ionization of the dopants and other low-temperature phenomena need to be taken into account by starting from the physics. While many models have been proposed so far for the V_T at low temperature, they are either semi-empirical, validated only down to moderate cryogenic temperature, or not accounting for the various physical phenomena contributing to the temperature

dependence of V_T [7]–[10]. For instance, the physics-based model from Jaeger and Fox [8] is valid down to 77 K and does not account for the dopant freezeout. Recently, Dao et al. [10] derived a V_T model valid down to 6 K by introducing two empirical parameters to account for the field-assisted ionization of the dopants. In this work, we demonstrate that both freezeout and field-assisted ionization are accounted for by a single incomplete-ionization term in the Poisson-Boltzmann equation. This results in an entirely physics-based, long-channel V_T model without introducing fitting parameters.

II. Cryogenic Measurements in 28-nm CMOS

Low-temperature measurements were performed in the four n-type width-over-length device-corners of a 28-nm bulk CMOS process. After cooling a Lakeshore CPX cryogenic probe station to its 4.2-K base temperature, the station was heated to 298 K with intermediate temperature steps at 20, 36, 50, 77, 110, 160, and 210 K. The transfer characteristics in linear ($V_{DS} = 5$ mV) and saturation ($V_{DS} = 0.9$ V) were acquired using a Keysight B1500A device analyzer. Temperature-variable probes were used on the bulk and source contact pads to ensure the same bulk reference at the different temperature steps. The measurements in saturation are shown in Fig. 1. V_T was extracted using a linear extrapolation method from the maximum transconductance and ΔV_T is shown in Fig. 2(a). For all devices, a monotonic V_T increase is obtained, leveling off in the deep cryogenic regime (below ≈ 50 K). The drain-induced barrier lowering (DIBL) [Fig. 2(b)] follows a similar trend and is highest for a narrow-long device.

III. Overview of V_T Temperature Dependences

We assume an n-type MOSFET with uniform acceptor doping density (N_A) in the silicon body [Fig. 3(a)]. The source and drain junctions can be assumed completely ionized at all temperatures due to impurity-band formation as a result of degenerate doping [9]. Based on the MOSFET band diagrams in Fig. 3, we discuss the physical phenomena that impact the V_T of a large MOSFET. The vacuum energy level (E_{vac}) is taken as the reference and a potential drop (ψ) is defined with respect to the intrinsic energy level E_i in the bulk ($E_{i,b}$), i.e., $\psi = -(E_i - E_{i,b})/q$, where q is the elementary charge.

1) Bandgap Widening and Scaling of Fermi-Dirac Occupation Function: The Si bandgap increases from ≈ 1.12 to 1.17 eV from 298 to 4.2 K, plotted in Fig. 4. The Fermi-Dirac occupation function $f(E)$ scales exponentially, approaching a step function at 4.2 K [compare $f(E)$ in Fig. 3(b) and (d)]. More band bending is required to generate sufficient overlap of $f(E)$ with the density-of-states (DOS) in the conduction band. Both phenomena will thus act to increase
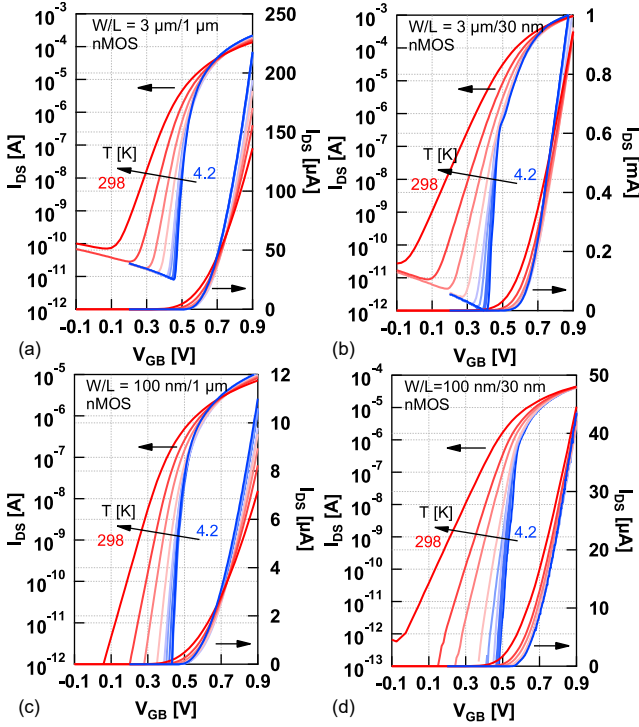
Fig. 1. Low-temperature measurements down to 4.2 K in a 28-nm CMOS process ($V_{DS} = 0.9$ V). In contrast with large devices (a), small devices (d) do not typically feature a cryogenic temperature-induced improvement of I_{ON} at $V_{DD} = 0.9$ V. Shifting the $I - V$ curve through technology optimization can solve this problem but requires accurate knowledge of V_T.
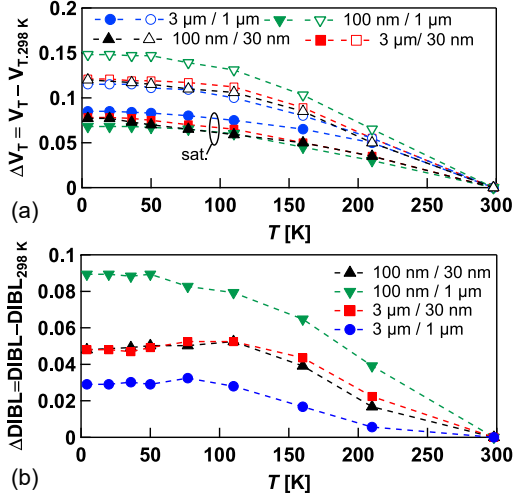

Fig. 2. a) Shift in V_T in saturation from Fig. 1 ($V_{DS} = 0.9$ V, filled markers) and linear ($V_{DS} = 5$ mV, open markers). b) DIBL versus temperature.

V_T. The effective masses and the DOS are assumed to have a negligible temperature dependence compared to $f(E)$ [7].

2) Intrinsic Carrier-Density Scaling: The Boltzmann statistics is validated for the deep-cryogenic temperatures [11]. The intrinsic carrier density (n_i) is thus given by the expression with exponential dependence on $-E_g$ and $1/T$. Respectively, the E_g widening and $f(E)$ scaling thus strongly decrease n_i.

3) Increase in Bulk Fermi-potential: The decrease in n_i is sufficiently strong to make the Fermi potential (assuming complete ionization) increase, given by $\Phi_F = U_T \ln(N_A/n_i)$ [Fig. 3(b) vs. 3(c)], despite its direct dependence on $U_T = kT/q$, the thermal voltage. Indeed, in order to satisfy charge neutrality in the case of a completely ionized N_A at 4.2 K [$p_p = n_i \exp(\Phi_F/U_T) = N_A$], E_F needs to lie very close to the valence band edge (E_v) to compensate for n_i [Fig.3(c)]. The increase in Φ_F ranges from about 0.1 V to 0.5 V depending on N_A, as shown by the dashed lines in Fig. 4. It can be checked that $\lim_{T\to 0 K} \Phi_F = E_g/2$. This increase in Φ_F constitutes a large portion of the V_T increase. However, the Φ_F increase is too strong and not sufficiently accurate. At 4.2 K, the silicon body would be degenerate ($E_g/2 - \Phi_F < 3kT$), which does not stroke with the measured electrical behavior in MOSFETs at 4.2 K. Incomplete ionization of N_A needs to be taken into account in the Fermi potential to avoid this.

4) Incomplete Ionization (thermal): Returning back to the charge neutrality, this gives $p_p = N_A^- = N_A f(E_A)$, where $f(E_A)$ is the ionization probability of the dopants, both due to temperature (thermal ionization) and the applied voltages (field-assisted ionization). Under charge neutrality, the field is zero and thus $f(E_A)$ equals the thermal ionization probability, given by $f_\theta = 1/\{1 + \alpha \exp[\Phi_F^* + V_{SB}]\}$, plotted in Fig. 6(b). Below $f_\theta \approx 20\%$, the silicon body will enter freezeout. At 4.2 K, incomplete ionization results in the position of E_F^* instead of E_F in Fig. 3(c), or mathematically:

$$\Phi_F^* = \underbrace{U_T \ln \frac{N_A}{n_i}}_{\Phi_F} - \underbrace{U_T \ln \frac{1 + \sqrt{1 + (4\alpha N_A)/n_i}}{2}}_{\Delta\Phi_F}, \quad (1)$$

where $\alpha = g_A \exp[(E_A - E_i)/(kT)] = g_A \exp(-\Phi_A/U_T)$. The acceptor potential $\Phi_A \triangleq (E_i - E_A)/q$ as well as Φ_F^* are shown in Fig. 4 with solid lines. The function $\Delta\Phi_F = \Phi_F - \Phi_F^*$ is plotted in Fig. 6(a) for different N_A and is in the order of millivolts. It can be checked that $\lim_{T\to 0 K} \Delta\Phi_F = \delta/2$ with $\delta = E_A - E_v = 0.045$ eV, for typical, hydrogen-like Si:B doping and thus $\lim_{T\to 0K} \Phi_F^* = \Phi_A + \delta/2$ as shown in Fig. 4. It might seem that $\Delta\Phi_F$ due to incomplete ionization is negligible for V_T at cryogenic temperatures compared to the overall increase of Φ_F or Φ_F^* in Fig. 4. However, Fig. 5 shows a large discrepancy in inverted density (n_p) at $2\Phi_F$ and $2\Phi_F^*$.

5) Incomplete Ionization (field): A second effect associated with the incomplete dopant ionization is the process of the frozen-out dopants ionizing due to the field, as shown by the band bending in Fig. 3(d). However, this field-assisted process of ionization (e.g., Poole-Frenkel [12]) happens in early depletion and is already completed near the surface before reaching the on-set of strong inversion where V_T is evaluated. This process can thus be possibly neglected in V_T and is not a justification for fitting parameters as done in [10].

IV. ANALYTICAL V_T MODEL

From standard MOS device physics it follows that the gate-to-bulk voltage is given by $V_{GB} = \psi_s + \Phi_{ms} + \varepsilon_{si}\mathcal{E}_s(\psi_s)/C_{ox}$, where ψ_s is the surface potential, ε_{si} the silicon permittivity,
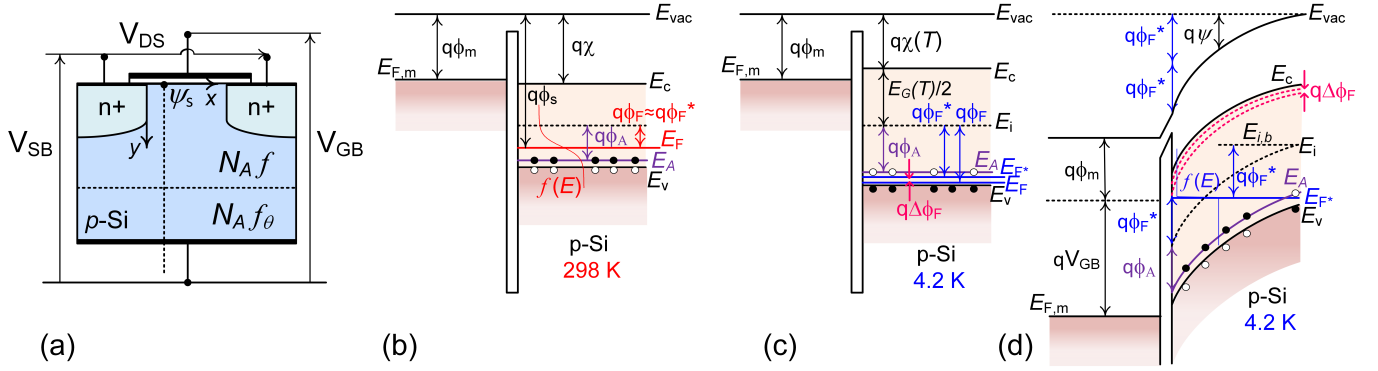
Fig. 3. a) Cross-section of an nMOSFET with incomplete ionization of N_A (thermal ionization probability given by f_θ. and thermal + field-assisted ionization given by f = Fermi-Dirac). Band diagrams from interface to bulk are shown: b) flat-band at 298 K, c) flat-band at 4.2 K ($p_p = N_A^-$ gives Φ_F^*, $p_p = N_A$ gives Φ_F), and d) strong-inversion threshold in the strict meaning ($n_p = N_A^-$). To reach this point, a band bending of $2q\Phi_F^*$ is needed when including incomplete ionization. An additional band bending over $q\Delta\Phi_F = q\Phi_F - q\Phi_F^*$ is needed to increase the inverted electron density from $n_p = N_A^-$ to $n_p = N_A$.

$\mathcal{E}_s$ the electric field normal to the semiconductor/oxide interface, C_{ox} the gate oxide capacitance, and Φ_{ms} the difference between the metal (Φ_m) and the semiconductor (Φ_s) work functions. Note that we do not take into account the oxide and interface-trapped charges. The threshold voltage is usually defined as the V_{GB} evaluated at a given value of ψ_s, i.e., the inversion threshold ψ_s', for which n_p equals the *totally ionized* N_A. Note that in the strict meaning of the inversion threshold when incomplete ionization is present, we have to define the threshold at $n_p = N_A^-$, since then the density of carriers in the channel has been inverted from the flatband case ($p_p = N_A^-$). However, this density can be very low due to freezeout and it is thus more meaningful to keep defining the threshold at $n_p = N_A$. The temperature dependence of the four terms of V_T are investigated separately below:

1) ψ_s': Near 298 K, the inversion threshold is taken at $2\Phi_F$ since then $n_p = N_A$ when complete ionization can be assumed. However, this threshold needs to be reassessed for the low and cryogenic temperatures. From $n_p = N_A$, we find that $\psi_s' = U_T \ln(N_A/n_i) + \Phi_F^* + V_{ch}(x) + V_{SB}$, where V_{ch} is the channel voltage. We evaluate V_T at source ($x = 0$) and assume $V_{SB} = 0$. It can be checked that this yields back $2\Phi_F$ for complete ionization ($\alpha = 0$). However, using (1), the correct inversion threshold is $\psi_s' = \Phi_F + \Phi_F^* = 2\Phi_F^* + \Delta\Phi_F = 2\Phi_F - \Delta\Phi_F$, and not $2\Phi_F$, nor $2\Phi_F^*$.

2) Φ_{ms}: From Fig. 3 we can obtain that $\Phi_{ms} = \Phi_m - (\chi + E_g/2 + \Phi_F^*)$. $E_{F,m}$ is assumed temperature independent due to metallic gate (or degeneracy in poly-Si). Due to lack of available data on the temperature dependence of χ in silicon down to 4.2 K, it is assumed that χ decreases with the same amount as E_g increases. Under these assumptions, the temperature dependence of Φ_{ms} is defined by Φ_F^*.

3) $\varepsilon_{si}\mathcal{E}_s(\psi_s')/C_{ox}$: The temperature dependences of ε_{si} and C_{ox} can be assumed negligible. From the Poisson-Boltzmann equation, $\partial^2 \psi(y)/\partial y^2 = -\rho(\psi)/\varepsilon_{si}$, including incomplete ionization, $\mathcal{E}_s$ in depletion can be derived as [11]: $\mathcal{E}_s = (U_T/L_D)\sqrt{\psi_s/U_T + \mathcal{F}}$, where ψ_s is the surface potential, $L_D = \sqrt{\varepsilon_{si}U_T/(2qN_A)}$, and $\mathcal{F}$ an extra term due to the incomplete ionization of N_A, given by $\mathcal{F} = \ln f_\theta +$
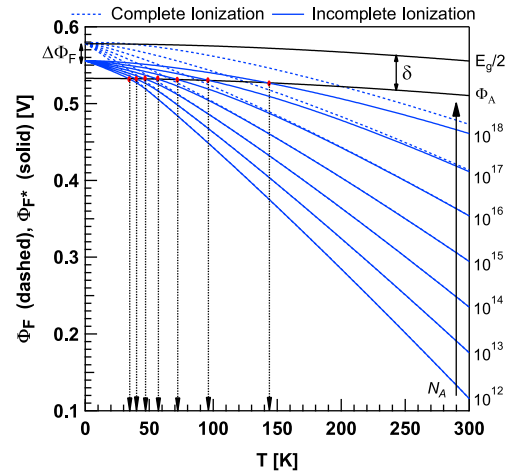

Fig. 4. Fermi potential in an nMOSFET as a function of T and N_A assuming complete ionization $[\Phi_F = U_T \ln(N_A/n_i)]$ versus incomplete ionization $[\Phi_F^*$ from (1)$]$. Freezeout of the p-type bulk happens when $\Phi_F^* \geqslant \Phi_A$ [= when $E_F^* \leqslant E_A$ in Fig. 3(c)]. Critical freezeout temperatures can be identified for given N_A at $\Phi_F^* = \Phi_A$. The difference between Φ_F and Φ_F^* is $\Delta\Phi_F$.

$\ln\{1 + \alpha \exp[(-\psi_s + \Phi_F^* + V_{ch} + V_{SB})/U_T]\}$. The second term, dependent on ψ_s, is due to the field-assisted ionization process. Evaluating $\mathcal{E}_s$ at $\psi_s' = 2\Phi_F - \Delta\Phi_F + V_{ch} + V_{SB}$ gives

$$\mathcal{E}_s(\psi_s') = \frac{U_T}{L_D}\sqrt{\frac{2\Phi_F - \Delta\Phi_F}{U_T} + \ln f_\theta + \ln\left(1 + \alpha e^{\frac{-\Phi_F}{U_T}}\right)}, \quad (2)$$

for $V_{ch} = V_{SB} = 0$. As evidenced by Figs. 6(c)-(d), the two logarithmic terms can be neglected tolerating a $\approx 1\%$ error on the electric field. This approximation can be viewed as neglecting the field-assisted ionization process which is completed at threshold ($\psi_s \gg 0$). Note that the different inversion threshold due to incomplete ionization, $2\Phi_F - \Delta\Phi_F$, is still taken into account. Considering all the temperature dependences together from the previous subsections, V_T is derived at the source as:

$$V_T = 2\Phi_F - \Delta\Phi_F + V_{SB} + \Phi_m' - \Phi_F^* + \Gamma_b\sqrt{2\Phi_F - \Delta\Phi_F + V_{SB}}. \quad (3)$$
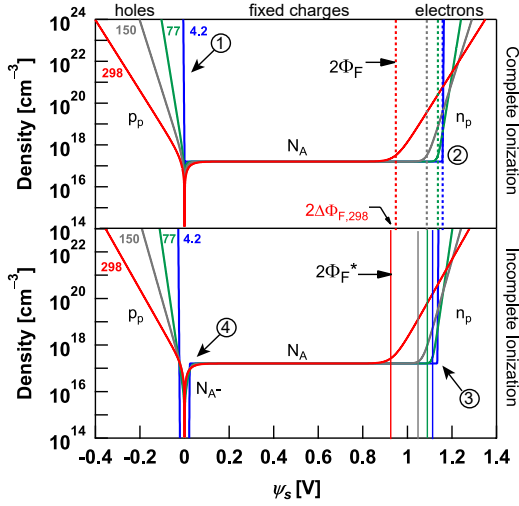
Fig. 5. Surface charge densities. (1) $f(E)$ scaling leads to a steeper turn-on of p_p in accumulation, and, similarly, of n_p in inversion. (2) Both $2\Phi_F$ and $2\Phi_F^*$ increase when temperature decreases. (3) The lower $2\Phi_F^*$ vs. $2\Phi_F$ is crucial at 4.2 K leading to a much lower inverted electron density. (4) Delayed turn-on of the fixed charges at 4.2 K due to the gate-voltage-dependent ionization of the frozen-out dopants. ($N_A = 10^{18}\,\mathrm{cm}^{-3}$, $V_{ch} = 0$).
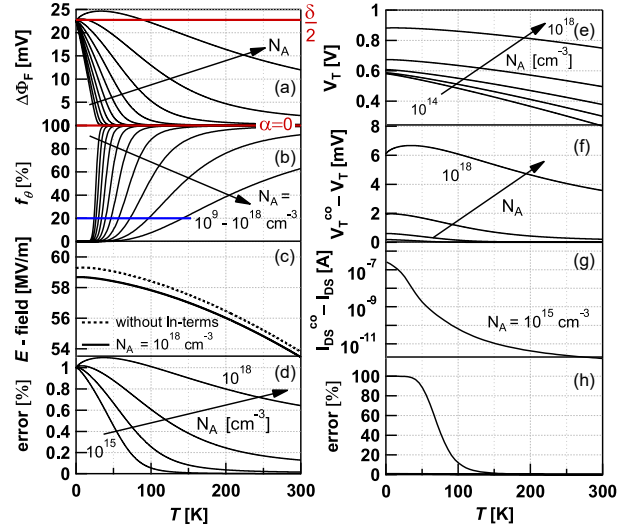

Fig. 6. a) $\Delta\Phi_F = \Phi_F - \Phi_F^*$, b) Thermal ionization probability of the dopants in flat-band and $V_{SB} = 0$. Complete ionization for $\alpha = 0$ and freezeout for $f_\theta \leqslant 20\,\%$. c)-d) $\mathcal{E}_s$ approximation without ln-terms. e) V_T from (3), f) Absolute error $V_T^{co} - V_T$, g)-h) Absolute and relative error on I_{DS}.
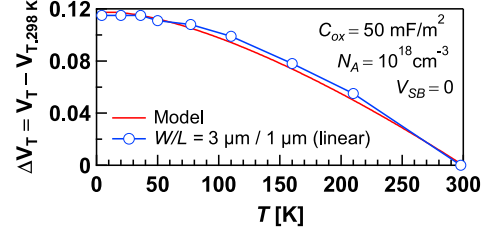
where $\Phi_m' = \Phi_m - (\chi + E_g/2)$ and $\Gamma_b = \sqrt{2qN_A\varepsilon_{si}}/C_{ox}$. It is now interesting to develop the error introduced by assuming complete ionization at all temperatures in (3) ($\Phi_F^* = \Phi_F$, $\Delta\Phi_F = 0$), reducing V_T to $V_T^{co} = V_T(\psi_s' = 2\Phi_F)$. The absolute error $V_T^{co} - V_T$ (note that $V_T^{co} > V_T$) is not large (millivolts) compared to a typical V_T at 4.2 K in a commercial device (≈ 0.4 V). However, due to the steepness of the subthreshold swing at 4.2 K, the absolute and relative error on the current are very large at cryogenic temperatures, as shown in Figs. 6(g) and 6(h). The current is considered in the linear regime, $I_{DS} = -(W/L)\mu Q_m V_{DS}$, and at constant mobility, μ, to illustrate this discrepancy. The used Q_m including incomplete ionization is given by

$$Q_m = -\gamma\sqrt{\frac{n_i}{N_A}\exp(\beta) + \frac{\psi_s}{U_T} + \mathcal{F}} + \gamma\sqrt{\frac{\psi_s}{U_T} + \mathcal{F}}, \quad (4)$$

where $\gamma = \varepsilon_{si}U_T/L_D$ and $\beta = (\psi_s - \Phi_F^* - V_{ch} - V_{SB})/U_T$. Fig. 7 validates the V_T model from (3) with the experimental results in a large nMOS at $V_{DS} = 5$ mV with negligible DIBL.

V. Conclusion

The increase of V_T down to 4.2 K is physically explained by E_g widening and Fermi-Dirac scaling. This leads to a strong decrease in n_i and thus increase in the inversion threshold $2\Phi_F$. Bulk incomplete ionization or freezeout makes the threshold $2\Phi_F - \Delta\Phi_F$, where $\Delta\Phi_F$ is temperature- and doping-dependent. Although in mV-range, $\Delta\Phi_F$ is significant for the cryogenic current. The process of field-assisted dopant ionization is negligible at inversion threshold. Good agreement is obtained between the V_T model and the experimental results.

Fig. 7. Model validation with experimental results in large nMOS.

References

[1] M. Veldhorst, C. Yang *et al.*, "A two-qubit logic gate in silicon," *Nature*, vol. 526, no. 7573, p. 410, 2015.

[2] L. Bourdet, L. Hutin *et al.*, "All-Electrical Control of a Hybrid Electron Spin/Valley Quantum Bit in SOI CMOS Technology," *IEEE Transactions on Electron Devices*, vol. 65, no. 11, pp. 5151–5156, Nov 2018.

[3] E. Charbon, F. Sebastiano *et al.*, "Cryo-CMOS for quantum computing," in *2016 IEEE IEDM*, Dec 2016, pp. 13.5.1–13.5.4.

[4] A. Beckers, F. Jazaeri *et al.*, "Cryogenic characterization of 28 nm bulk CMOS technology for quantum computing," in *2017 47th European Solid-State Device Research Conference (ESSDERC)*, pp. 62–65.

[5] A. Beckers, F. Jazaeri, and C. Enz, "Characterization and Modeling of 28-nm Bulk CMOS Technology Down to 4.2 K," *IEEE Journal of the Electron Devices Society*, vol. 6, pp. 1007–1018, 2018.

[6] A. Beckers, F. Jazaeri *et al.*, "Characterization and modeling of 28-nm FDSOI CMOS technology down to cryogenic temperatures," *Solid-State Electronics*, 2019.

[7] E. A. Gutierrez-D, J. Deen, and C. Claeys, "Low temperature electronics: physics, devices, circuits, and applications," *Elsevier*, 2000.

[8] R. M. Fox and R. C. Jaeger, "MOSFET behavior and circuit considerations for analog applications at 77 K," *IEEE T-ED*, vol. 34, 1987.

[9] A. Akturk, J. Allnutt *et al.*, "Device modeling at cryogenic temperatures: Effects of incomplete ionization," *IEEE T-ED*, vol. 54, no. 11, 2007.

[10] N. C. Dao, A. E. Kass *et al.*, "An enhanced MOSFET threshold voltage model for 6–300K temperature range," *Microelectron. Reliability*, 2017.

[11] A. Beckers, F. Jazaeri, and C. Enz, "Cryogenic MOS Transistor Model," *IEEE Trans. on Electron Devices*, vol. 65, no. 9, pp. 3617–3625, 2018.

[12] D. P. Foty, "Impurity ionization in MOSFETs at very low temperatures," *Cryogenics*, vol. 30, no. 12, pp. 1056 – 1063, 1990.